Critical Behaviors of Asymmetric Granular Maxwell's Demon Phenomenon

Yota Nonaka* and Syuji Miyazaki†

Graduate School of Informatics, Kyoto University, Kyoto, 606-8501, Japan

We theoretically derived the critical behaviors of the asymmetric granular Maxwell's demon phenomenon by introducing a symmetry-breaking parameter. This symmetry breaking can be realized experimentally by forming an angle between the vibration and vertical directions. The values of the conventional critical exponents β, γ, and δ were determined, and they satisfied Widom's scaling relation. In addition, the scaling function was calculated using asymptotic expansion, which was consistent with the numerical simulation.

1. Introduction

Sand as Maxwell's Demon written by Jens Eggers describes a dilute gas of granular material inside a box, in which a wall separates the box into two identical compartments except for a small hole at some finite height, kept in a stationary state by vertical vibrations, and the particles preferentially occupy one side of the box at a suitable vibration intensity.[1)] He analyzed this clustering phenomenon on the basis of a thermodynamical approach to the granular material and constructed a mean-field model.[1)] Schlichting and Nordmeier described the first experimental implementation.[2)] A generalization from a single dispersion to a double dispersion in radius was analyzed to yield a granular clock.[3)] Another generalization was an asymmetry, which corresponds to an external magnetic field in the magnetic phase transition. In one generalization, a simple hole was replaced by a funnel.[4)] In another generalization, the floor of one of the two compartments was raised.[5,6)] These generalizations enhanced the asymmetric flux through a hole or a funnel. Such asymmetry-induced transitions and related critical phenomena have not been analyzed thus far. An important preceding study was on the critical behaviors described by a cellular automaton traffic flow model using an order parameter breaking the symmetry of the jam-free phase, in which conventional critical exponents satisfy a scaling relation.[7)] Phase transitions and critical phenomena of compartmentalized granular gases have been studied and reviewed from various aspects up to now.[8–15)]

Critical phenomena are universally found in many systems where a second-order phase transition is observed. One of the most representative systems is van der Waals gases, for which the critical exponents are $\beta = 1/2$, $\gamma = 1$, and $\delta = 3$. The Ising model is also a well-known system that demonstrates phase transition and critical behavior. When the Ising model is analyzed under the mean-field approximation, the critical exponents have the same values as those of van der Waals gases. These common values can also be derived from the broader framework of Landau theory and are called the classical values of critical exponents.

Systems exhibiting critical phenomena are not limited to models in physics. For example, the equilibrium value of a stock in a market that allows a negative price also exhibits a phase transition, which explains the anomalous price over earnings ratio commonly seen in the market.[16)] As another example, traffic congestion commonly observed in daily life is actively examined as a target of statistical physics. In these studies, the transition from uncongested to congested was regarded as a phase transition. Introducing an asymmetry parameter termed random braking makes it possible to calculate the critical exponents and the scaling function numerically.[7)] We introduced a symmetry-breaking parameter θ to the granular Maxwell's demon phenomenon,[1)] and this extension enabled us to derive the critical exponents and the scaling function.

This paper is organized as follows: In the next section, we describe the granular Maxwell's demon phenomenon, thermodynamical treatment of the granular particles, and its temperature uniformity approximation. Dynamics of the biased number density were derived and the bias in the equilibrium state was clarified. Then, we implemented a tilted container in order to describe a symmetry-breaking transition. Scaling exponents and scaling functions were theoretically derived and compared with the numerical simulation.

2. Granular Maxwell's Demon and Its Tilted Equipment

2.1 Thermodynamical treatment of granular particles

We prepared granular particles in two evenly separated areas of a container. The separator has a hole that enables the particles to move from one compartment to the other. The base end surface is vertically oscillating in a sawtooth waveform with the amplitude U, such that the end surface always collides with the particles at the same speed U. We assumed that the particles cannot reach the ceiling, that the interparticle restitution coefficient e satisfies $e \lesssim 1$, and that the particles elastically collide with the container side surface. Imagine the case of $\theta = 0$ in Fig. 1.

Starting from a uniform distribution of the particles, the particles aggregated in one compartment over time, under the condition that the height of the hole h from the end surface was larger than the threshold h_c. As this phenomenon resembled Maxwell's demon, we termed it granular Maxwell's demon.

An intuitive explanation is as follows. An instantaneous fluctuation causes the number of particles in, for example, the right area to become larger than that in the left. Then in the right area, when the particle number becomes larger, inelastic collisions occur more frequently, such that the particles less frequently reach the hole owing to the dissipation of kinetic energy. In contrast, the particles in the left area reach the hole more frequently owing to a relative increase in kinetic

energy, because the interparticle collisions become less frequent. Thus, the flux from the right area to the left decreases and that from the reverse direction increases. The difference in number is increased by positive feedback. The left-hand-side aggregation is explained in the same manner. The aggregated side is highly dependent on initial fluctuations. We briefly review the thermodynamical treatment in accordance with Eggers's work.[1)]

We first treated a system consisting of a box with width W and N granular particles. The particles with radius r and mass m collide with a coefficient of normal restitution e. This wall has a small hole at height h through which particles can pass to the other side. The width of the hole was $2l$, where l is the radius of the hole.

The box is mounted on a shaker with a bottom vibration pattern with a sawtooth amplitude function; therefore, the velocity U of the bottom is constant. Particles accelerated by gravity g bounce back on the floor and gain energy. The x- and y-axes correspond to the horizontal and vertical directions, respectively, where y is equal to 0 at the base surface.

When we regarded the granular particles as fluid, we defined pressure $P(y)$, temperature $T(y)$, and particle number density per unit width $n(y)$ as functions of the height y of the particle. The temperature can be considered as the mean kinetic energy of the particle in a small region. The basic equations away from the base end surface consisting of the state equation, the balance equation of the forces, and the balance equation between heat flow and dissipation[17)] are

$$P = mnT, \tag{1}$$

$$\frac{\partial P}{\partial y} = -mgn, \tag{2}$$

$$\kappa \frac{\partial}{\partial y}\left[T^{1/2}\frac{\partial T}{\partial y}\right] = Dn^2T^{3/2}, \tag{3}$$

respectively, where the parameters κ and D are given by

$$\kappa = \frac{m}{\sqrt{\pi}r}, \tag{4}$$

$$D = 4\sqrt{\pi}mr(1-e), \tag{5}$$

where the velocity U of the end surface appears explicitly not in these equations but in the boundary condition of the temperature T.

2.2 Temperature uniformity approximation

We approximated the temperature uniformity, that is, the temperature $T(y)$ was independent of height y and constant, yielding an analytical result. Under this approximation, the balance equation Eq. (3) no longer holds. Equations (1) and (2) yield

$$n(y) = \frac{\tilde{N}mg}{T}\exp\left(-\frac{mgy}{T}\right). \tag{6}$$

The assumption that T is constant, which is independent of y, implies that the velocity distribution $q(u, v)$ obeys

$$q(u,v) = \frac{m}{2\pi T}\exp\left(-\frac{m(u^2+v^2)}{2T}\right), \tag{7}$$

where u and v are horizontal and vertical components, respectively.

However, the energy dissipation D and the energy influx S due to the collisions on the end surface are respectively given by[17)]

$$D = \sqrt{\pi}r\tilde{N}^2 g\sqrt{mT}(1-e^2), \tag{8}$$

$$S = \frac{\tilde{N}mg}{T}\left(TU + 2\sqrt{\frac{2}{\pi}mT}U^2 + O(mU^3)\right). \tag{9}$$

The balance equation between D and S determines the temperature T. Note that Eq. (9) holds under the condition $mU^2 \ll T$, which suggests that the kinetic energy of the particle is much larger than the energy gain owing to the collision on the end surface. For example, a larger restitution coefficient e corresponds to this condition, under which the second term on the right-hand side of the expression of S can be negligible giving

$$T = \frac{mU^2}{\pi\tilde{N}^2r^2(1-e^2)^2}. \tag{10}$$

2.3 Dynamics of biased number density

Using the above results for granular systems in a box, we derived the dynamics of the bias parameter in the granular Maxwell's demon phenomenon. N_l and N_r are the numbers of particles on the left and right sides, respectively. The number of particles per unit width was defined by $\tilde{N}_\mathrm{l} = N_\mathrm{l}/W$ and $\tilde{N}_\mathrm{r} = N_\mathrm{r}/W$. Therefore, the temperatures T_l and T_r for the left and right areas, respectively, were calculated as

$$T_\mathrm{i} = \frac{mU^2}{\pi\tilde{N}_\mathrm{i}^2r^2(1-e^2)^2}, \tag{11}$$

where i is a subscript representing r or l. Thus, we calculated the particle density $n_\mathrm{i}(y)$ and velocity distribution $q_\mathrm{i}(u, v)$ in compartment i. We defined

$$\epsilon = \frac{2N_\mathrm{l} - N}{2N} \tag{12}$$

as a parameter that represents the bias in the number of particles. The dynamics of ϵ can be described as

$$\frac{d\epsilon}{dt} \propto F_{\mathrm{r}\to\mathrm{l}} - F_{\mathrm{l}\to\mathrm{r}} \tag{13}$$

using the fluxes (i.e., the number of particles passing per unit time) $F_{\mathrm{l}\to\mathrm{r}}$ and $F_{\mathrm{r}\to\mathrm{l}}$ at height h. Note that $F_{\mathrm{l}\to\mathrm{r}}$ is given by

$$F_{\mathrm{l}\to\mathrm{r}} = n_\mathrm{l}(h)\int_0^\infty du\int_{-\infty}^\infty q_\mathrm{l}(u,v)dv. \tag{14}$$

Substituting Eqs. (6) and (7) gave

$$\frac{d\epsilon}{dt} \propto \tilde{N}_\mathrm{l}^2\exp\left(-\frac{mgh}{T_\mathrm{l}}\right) - \tilde{N}_\mathrm{r}^2\exp\left(-\frac{mgh}{T_\mathrm{r}}\right). \tag{15}$$

Furthermore, from Eq. (11), the exponential part, $\dfrac{mgh}{T_\mathrm{i}}$, was transformed as follows:

$$\frac{mgh}{T_\mathrm{i}} = mgh\frac{\pi\tilde{N}_\mathrm{i}^2r^2(1-e^2)^2}{mU^2} \simeq \frac{4\pi gh\tilde{N}_\mathrm{i}^2r^2(1-e)^2}{U^2}. \tag{16}$$

However, e was assumed to be sufficiently large, $e \lesssim 1$, and we used the relation $1 + e \simeq 2$. By introducing the dimensionless parameter

$$\mu = \frac{4\pi gh}{U^2}\left(\frac{rN}{W}\right)^2(1-e)^2, \tag{17}$$

the dynamics of the system were simplified to

$$\frac{d\epsilon}{dt} \propto (\epsilon - \frac{1}{2})^2 \exp\left(-\mu(\epsilon - \frac{1}{2})^2\right) - (\epsilon + \frac{1}{2})^2 \exp\left(-\mu(\epsilon + \frac{1}{2})^2\right). \quad (18)$$

The condition for the system to be in a steady state is given by $\frac{d\epsilon}{dt} = 0$, which means that $\epsilon(\mu)$ can be calculated from Eq. (18). Expanding Eq. (18) for small ϵ, we obtained

$$\epsilon = \sqrt{\frac{3(\mu - 4)}{16}} \quad (19)$$

as the behavior near the critical point. When we regarded this phenomenon as a phase transition with spontaneous symmetry breaking, it was a second-order transition with the critical exponent $\beta = 1/2$.[1)]

The U dependence of temperature T in Eq. (10) sensitively relies on the mechanism of dissipation of inelastic collisions or viscous drag and also on whether the amplitude function for the velocity of the vibrating surface is symmetric (sinusoidal) or asymmetric (sawtooth) about zero velocity, and the coefficient multiplied by U^2 in the right-hand side differs for other mechanisms of dissipation or other amplitude functions for the velocity of the vibrating surface.[17)] Nonetheless, the critical behavior (critical exponents, scaling function, etc.) around the critical condensation point is assumed to be independent of the detailed features of the system even for the simplified flux equation. According to Eggers,[1)] the agreement between Eqs. (1)–(3) and the numerical simulation is quite good, but becomes worse if the number of particles is reduced and deteriorates even more in three dimensions.

2.4 Tilted implement

Several studies have been performed to introduce asymmetric structures into the phenomenon of Maxwell's demon in granular matter. For example, directed clustering was attempted by making a funnel-shaped hole[4)] or by adding a slab into one of the compartments.[5,6)] On the other hand, critical phenomena for the asymmetric case have not been investigated. We present theoretical results using a tilted vessel and derived the critical phenomena.

As shown in Fig. 1, we considered the one-sided aggregation of granular particles when the container is tilted at a small angle θ. When the coordinate axes were set as shown in Fig. 1, the gravitational acceleration was represented by the vector $\mathbf{g} = (-g\sin\theta, -g\cos\theta)$ such that Eq. (6), which gives the particle density, becomes

$$n(x, y) \propto \exp\left(\frac{mg\sin\theta}{T}x\right)\exp\left(\frac{mg\cos\theta}{T}y\right), \quad (20)$$

where the granular temperature is given by Eq. (10). Performing the same analysis as when the vessel was not tilted, we obtained the flux ratio

$$\begin{aligned} & F_{\mathrm{l}\to\mathrm{r}} : F_{\mathrm{r}\to\mathrm{l}} \\ = \; & n_{\mathrm{l}}\left(\frac{W}{2}, h\right)\int uq_{\mathrm{l}}(u, v)dudv \\ & : n_{\mathrm{r}}\left(-\frac{W}{2}, h\right)\int uq_{\mathrm{r}}(u, v)dudv \end{aligned}$$

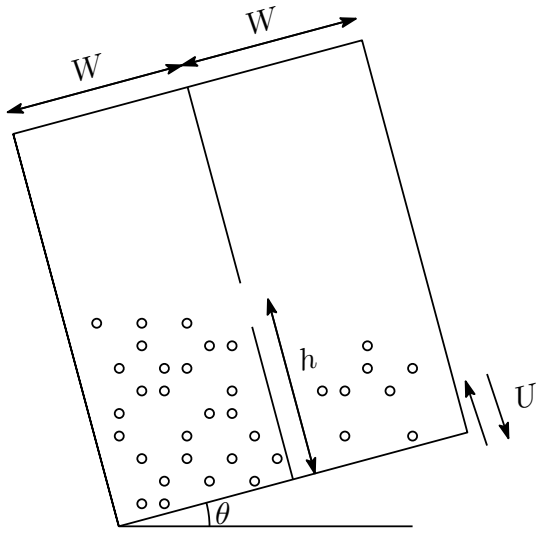

Fig. 1. Tilted implement of granular Maxwell's demon.

$$= \frac{N_{\mathrm{l}}}{\sqrt{T_{\mathrm{l}}}}\exp\left(-\frac{mgh\cos\theta}{T_{\mathrm{l}}}\right) : \frac{N_{\mathrm{r}}}{\sqrt{T_{\mathrm{r}}}}\exp\left(-\frac{mgh\cos\theta - mgW\sin\theta}{T_{\mathrm{r}}}\right). \quad (21)$$

Therefore, we altered the dynamics of ϵ to

$$\frac{d\epsilon}{dt} \propto (\epsilon - \frac{1}{2})^2 \exp\left(-\mu(\epsilon - \frac{1}{2})^2\right) - (\epsilon + \frac{1}{2})^2 \exp\left(-\mu(\epsilon + \frac{1}{2})^2(1 - p)\right), \quad (22)$$

where we introduced $p = \frac{W\sin\theta}{h}$ representing asymmetry, which was proportional to θ for the small tilted angle. Then, the stationary equation became

$$(\epsilon - \frac{1}{2})^2 \exp\left(-\mu(\epsilon - \frac{1}{2})^2\right) = (\epsilon + \frac{1}{2})^2 \exp\left(-\mu(\epsilon + \frac{1}{2})^2(1 - p)\right). \quad (23)$$

This equation yielded the order parameter $\epsilon(\mu, p)$ in the steady state. Note that if $\mu > \mu_c = 4$, the nonzero solution $\epsilon = \epsilon(\mu, p)$ becomes stable. The critical behaviors for the extended model were expected to obey the following power laws:

$$\epsilon(\mu, 0) \sim (\mu - \mu_c)^{\beta}, \quad (24)$$

$$\epsilon(\mu_c, p) \sim p^{1/\delta} \sim \theta^{1/\delta}, \quad (25)$$

$$\chi(\mu) \sim |\mu_c - \mu|^{-\gamma}, \quad (26)$$

where χ is the susceptibility defined by $\chi = \left.\frac{\partial\epsilon}{\partial p}\right|_{p=0}$. As ϵ is sufficiently small just above the critical point $\mu = \mu_c, \beta = 1/2$, $\gamma = 1$, and $\delta = 3$ were obtained using an asymptotic expansion. Note that these are classical values of critical exponents obtained from Landau theory and satisfy the following Widom's scaling relation:

$$\gamma = \beta(\delta - 1). \quad (27)$$

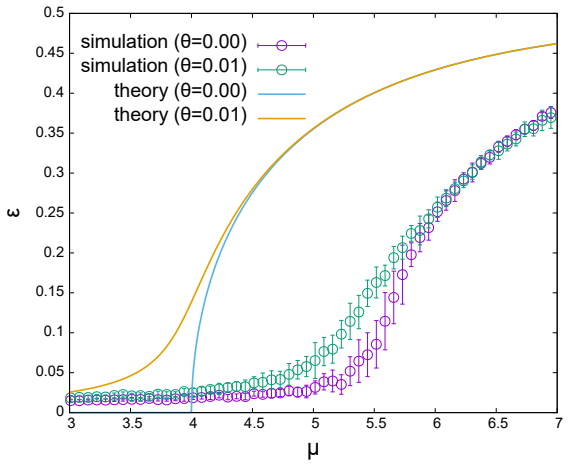

Fig. 2. (Color online) Results of numerical simulation and theoretical analysis Eq. (23) of the bias $\epsilon(\mu, p)$ at equilibrium. "theory" is the result of the calculation under the temperature uniformity approximation. The upper and lower lines correspond to the simulations for $\theta = 0$ and $\theta = 0.01$, respectively. The upper and lower symbols with error bars correspond to the theory for $\theta = 0$ and $\theta = 0.01$, respectively.

Therefore, Widom's scaling hypothesis was expected to hold true:

$$\epsilon = |\mu - \mu_c|^{\beta}\tilde{\epsilon}\left(\frac{p}{|\mu - \mu_c|^{\beta\delta}}\right) \sim |\mu - \mu_c|^{\beta}\tilde{\epsilon}\left(\frac{W\theta}{h|\mu - \mu_c|^{\beta\delta}}\right). \quad (28)$$

Near the critical point, condition (23) yields the equation that $\tilde{\epsilon}(x)$ must satisfy:

$$\tilde{\epsilon}(x)^3 \pm \frac{3}{16}\tilde{\epsilon}(x) - \frac{3}{32}x = 0, \quad (29)$$

where $x = \dfrac{p}{|\mu - \mu_c|^{\beta\delta}} \sim \dfrac{W\theta}{h|\mu - \mu_c|^{\beta\delta}}$. The sign of the second term was positive (negative) when $\mu < \mu_c$ ($\mu > \mu_c$).

The bias ϵ at equilibrium was calculated as a function of the normalized hole height μ, by the event-driven method,[18] as shown in Fig. 2. The simulation parameters are listed in Table I and are used for the simulation and calculation of the analytical solution where the end surface was tilted at angle $\theta = 0.01$. In the simulations, 20 samples were taken for each value of hole height μ, and the bias ϵ was measured at the elapsed time $t = 6000$ unit of the simulation, which is sufficient for the system to relax, based on Eq. (12), and the variance is shown as error bars in the graph. As shown in Fig. 2, Eq. (23) reproduced the approximate behaviors.

To calculate the critical exponents, three simulations were conducted. For the first step, the critical value μ_c was determined on the basis of the divergence of χ. The value of χ was calculated approximately as $\chi \simeq \lim_{p\to 0} \dfrac{\epsilon(p) - \epsilon}{p - 0}$. From this simulation, the critical point was $\mu_c = 5.40$. As a result, we found $\gamma = 1.040 \pm 0.041$ by plotting the results on a double-logarithmic graph for $\theta = 0.01$, as shown in Fig. 3. As the second step, $\beta = 0.471 \pm 0.058$ was determined by setting $p = 0$ ($\theta = 0$) near the critical point, as shown in Fig. 4. Lastly, the dependence of ϵ on θ at the critical point $\mu = \mu_c$ was clarified as $\delta = 3.341 \pm 0.460$, as shown in Fig. 5. These values were consistent with the results of analyses based on the flux model.

For each case of $\mu < \mu_c$ and $\mu > \mu_c$, the scaling functions

Table I. Parameter list.

N	m	r	e	g	W	U	$2l$
720	1	0.01	0.95	1	3.2	0.149	0.05

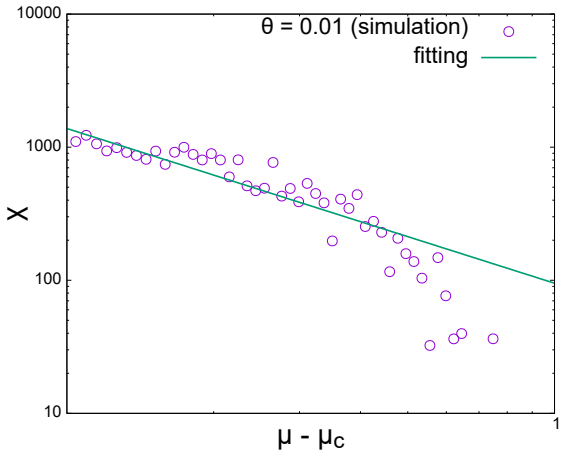

Fig. 3. (Color online) Double-logarithmic plot of ϵ against $\mu - \mu_c$ for $\theta = 0.01$. The critical exponent γ was estimated as $\gamma = 1.040 \pm 0.041$.

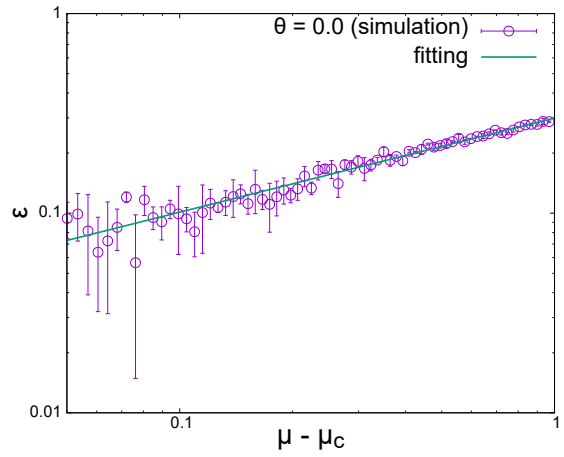

Fig. 4. (Color online) Double-logarithmic plot of ϵ against $\mu - \mu_c$ for $\theta = 0$. The critical exponent γ was estimated as $\beta = 0.471 \pm 0.058$.

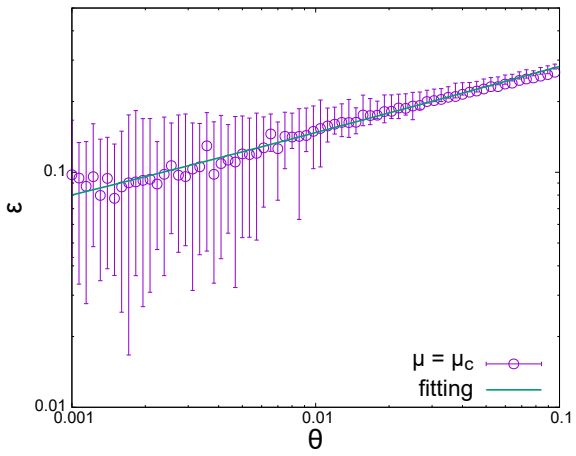

Fig. 5. (Color online) Double-logarithmic plot of ϵ against θ. The critical exponent δ was estimated as $\delta = 3.341 \pm 0.460$.

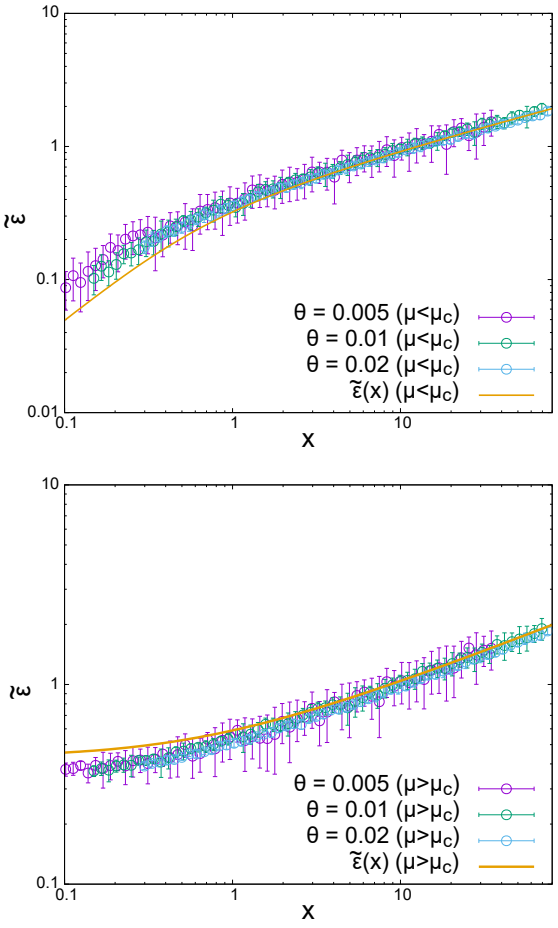

Fig. 6. (Color online) Scaling functions $\tilde{\epsilon}$ of the numerical simulation and analytical solution. From the scaling analysis, the critical point was determined, such that the data lie on the same curve for all θ, which in this case is $\mu_c = 5.44$. (upper) $\mu < \mu_c$. (lower) $\mu > \mu_c$.

$\tilde{\epsilon} = \dfrac{\epsilon}{|\mu - \mu_c|^{\beta}}$ as a function of $x = \dfrac{p}{|\mu - \mu_c|^{\beta\delta}} \sim \dfrac{W\theta}{h|\mu - \mu_c|^{\beta\delta}}$ with $(\beta, \gamma, \delta) = (1/2, 1, 3)$ for three values of θ (θ =0.005, 0.01, and 0.02) were plotted as shown in Fig. 6. Theoretical estimations based on the temperature uniformity approximation of the critical exponents $(\beta, \gamma, \delta) = (1/2, 1, 3)$ and of the scaling function $\tilde{\epsilon}(x)$ were numerically confirmed, as shown in Fig. 6.

3. Concluding Remarks

There was a large difference in the critical points between the temperature uniformity approximation ($\mu_c = 4$) and the numerical simulation ($\mu_c = 5.44$), which was also observed in the preceding study.[1)] We infer that the discrepancy between $\mu_c = 4$ for the theoretical estimation and $\mu_c = 5.40$ for the numerical simulation originates from the violation of the temperature uniformity approximation around the end surface. P, n, and T of Eqs. (1)–(3) can be expanded as series of y. For example, $T(y) = T(0) - ay + by^2 + \cdots$ ($a > 0$). One can interpolate between a solution around the end surface and the asymptotic value $T(\infty)$ by using an exponential function as $T(y) = (T(0) - T(\infty)) \exp(-\frac{ay}{T(0)-T(\infty)}) + T(\infty)$. The temperature uniformity approximation adopted only the second term $T(\infty)$. The first term $(T(0) - T(\infty)) \exp(-\frac{ay}{T(0)-T(\infty)})$ may fill a gap of the critical point between the temperature uniformity approximation and the numerical simulation. We will study this point in the future.

We obtained the distribution functions of u, i.e., $q(u) = \int_{-\infty}^{\infty} q(u, v)dv$, and of v, i.e., $q(v) = \int_{-\infty}^{\infty} q(u, v)du$ for $\theta = 0$, as shown in Fig. 7, where $q(v)$ exhibits a slight asymmetric deviation from the Maxwellian owing to the end surface oscillation. The seventh annotation of van der Weele's review[12)] claimed that *recent experiments suggest that this identification ($T_g = \frac{1}{2}\langle v^2 \rangle$) holds quite generally for vibrated granular gases of identical particles, and that (except for the bottom layer) the velocity distribution is very nearly Maxwellian throughout the system*. One of the above experiments was a two-layer granular experiment, in which velocity statistics of the first- and second-layer grains were obtained. The former was non-Gaussian, and the latter was almost Gaussian in the sense that the values of $|F - 3|$ ran from 0.01 to 0.1 for the latter and were nearly equal to 1 for the former, where F is the flatness, $\langle v^4 \rangle / \langle v^2 \rangle^2$, and is equal to 3 for a Gaussian distribution.[10)] In our case, the flatness is equal to 2.86 (2.95) for the vertical (horizontal) velocity component, which corresponds to the lower (upper) panel of Fig. 7. This finding validates the temperature uniformity approximation aside from the lower particles directly touching the end surface. The flatness of the distribution $q(v)$ is close to that of the second layer of the above experiment.[10)] We also calculated the skewness, $\langle v^3 \rangle / \langle v^2 \rangle^{3/2}$, which is equal to 0.156 (0.00193) for the vertical (horizontal) velocity component. The skewness in a different situation was studied.[19)] Although the distribution $q(v)$ was not given, y dependences of the temperature $T(y)$ were obtained in the preceding studies,[1,12)] where the temperature was not constant around the end surface. Systematic discrepancies of the scaling function $\tilde{\epsilon}(x)$ for small x between the temperature uniformity approximation and the numerical estimation, as shown in Fig. 6, are also inferred to originate from the violation of the temperature uniformity approximation around the end surface. An inverse power-law dependence on velocity in the velocity distribution was found in the case of a dilute limit with dissipation due to viscous drag, and our case was treated as Maxwellian.[17)]

The areal velocity of the end surface is $WU = WA\omega/(2\pi)$, and the period of the vibration is $2\pi/\omega$, where A is the amplitude of the sawtooth floor vibration. Thus, the area of the range of motion of the end surface is $2\pi WU/\omega = WA$. The total area of the particles in this area is $\pi r^2 Nn(0)$. The dilute condition around the end surface is estimated as $WA \gg \pi r^2 Nn(0)$ or $\pi r^2 Nn(0)/(WA) \ll 1$. The values of the parameters are given in Table I. In our numerical simulation, $n(0)$ is nearly equal to 0.7, and $\pi r^2 Nn(0)/(WA)$ is nearly equal to $4.948/A$. Since the velocity component of the particles normal to the end surface is always U after the collision with it, the explicit value of A is not used in the simulation and is assumed to be very small. It implies that the dilute condition is not satisfied in the vicinity of the end surface, but it is satisfied with increasing distance from the end surface.

The flux equation Eq. (18) has a wide application. An application to the consensus formation with the prospect theory was made.[20)]

In summary, we introduced a symmetry-breaking parameter θ, which enabled us to calculate critical exponents β, γ, and δ. The theoretical analyses based on the flux model and

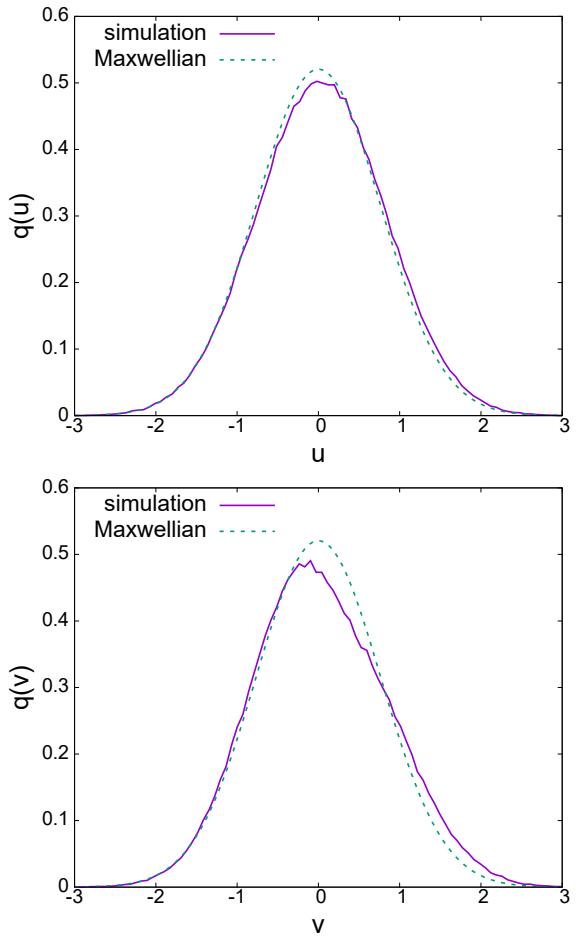

Fig. 7. (Color online) Distributions of the horizontal (upper panel) and vertical (lower panel) velocity components. The Maxwell distribution and the numerically obtained distribution are respectively depicted as a dashed line and a solid line.

numerical simulations demonstrated that these values satisfy Widom's scaling relation $\gamma = \beta(\delta-1)$, and the scaling function calculated using asymptotic expansion corresponded reasonably well to the simulated data.

One reason why the critical exponents obtained by the simulations agreed with the classical critical exponents is the Landau theory, which exhibits symmetry breaking and the classical critical exponents of a system obeying dynamics, such as Eq. (22). Therefore, the critical exponents being classical suggests that an essential part of the system is represented by the flux model Eq. (22). Thus, the state of the system was sufficiently condensed into the order parameter and did not depend on the detailed configuration of the particles. This system had a high coefficient of restitution ($e = 0.95$) and was close to thermal equilibrium; therefore, the above condition held true. The determination of the conditions required for the system to be *mean-field*, i.e., for the information of the system to be reduced to an order variable, is a future challenge. It is also important to note that such results may be derived in a setting that is experimentally possible and follow-up experiments are awaited. Of note, this system is dissipative and therefore not at equilibrium. It is important to note that nonequilibrium phase transitions can be described in a mean-field manner, and the conditions under which mean-field analysis is possible must be examined in greater detail.

Acknowledgment

We would like to thank Masaharu Isobe for advising us on the numerical simulation.

1) J. Eggers, Phys. Rev. Lett. **83**, 5322 (1999).
2) H. J. Schlichting and V. Nordmeier, Math. Naturwiss. Unterr. **49**, 323 (1996) [in German].
3) R. Lambiotte, J. M. Salazar, and L. Breni, Phys. Lett. A **343**, 224 (2005).
4) F. Corrales, Y. Nahmad, and E. Altshuler, Rev. Cubana Fís. **35**, 50 (2018).
5) Y. Zhang, Y.-C. Li, R. Liu, F.-F. Cui, P. Evesque, and M.-Y. Hou, Chin. Phys. B **22**, 054701 (2013).
6) Y. Li, M. Hou, and P. Evesque, J. Phys. Conf. Ser., **327**, 012034 (2011).
7) N. Boccara and H. Fuks, J. Phys. A **33**, 3407 (2000).
8) A. W. Alexander, T. Shinbrot, and F. J. Muzzio, Phys. Fluids **13**, 578 (2001).
9) R. Mikkelsen, K. van der Weele, D. van der Meer, M. van Hecke, and D. Lohse, Phys. Rev. E **71**, 041302 (2005).
10) G. W. Baxter and J. S. Olafsen, Granular Matter **9**, 135 (2007).
11) X. Liu and P. Tong, Chinese Phys. B **17**, 3930 (2008).
12) K. van der Weele, Contemporary Physics **49**, 157 (2008).
13) G. Kanellopoulos and K. van der Weele, Phys. Rev. E **85**, 061303 (2012).
14) F. Chung and S. Liaw, Granular Matter **15**, 57 (2013).
15) G. Gotti, S. Iubini, and P. Politi, Phys. Rev. E **103**, 052133 (2021).
16) D. Sornette, Physica A **284**, 355 (2000).
17) V. Kumaran, Phys. Rev. E **57**, 5660 (1998).
18) M. Isobe, International Journal of Modern Physics C **10**, 1281 (1999).
19) C. Yanpei, P. Evesque, M. Hou, C. Lecoutre, F. Palencia, and Y. Garrabos, Journal of Physics: Conference Series **327**, 012033 (2011).
20) Y. Nonaka and S. Miyazaki, J. Phys. Soc. Jpn. **90**, 104803 (2021).